Journal of ELECTRONIC MATERIALS, Vol. 46, No. 8, 2017
DOI: 10.1007/s11664-017-5526-5

$Ni(OH)_2$ Aerogels Incorporated with Polypyrrole as Electrodes for Supercapacitors

LETÍCIA T. SCARABELOT,[2] DALIANA MULLER,[1] LUCIANA V. DE SOUZA,[1] DACHAMIR HOTZA,[1,3] and CARLOS R. RAMBO[1,2,4]

1.—Graduate Program on Materials Science and Engineering (PGMAT), Federal University of Santa Catarina (UFSC), Florianópolis, SC 88040-900, Brazil. 2.—Department of Electrical and Electronic Engineering (EEL), Federal University of Santa Catarina (UFSC), Florianópolis, SC 88040-900, Brazil. 3.—Department of Chemical and Food Engineering (EQA), Federal University of Santa Catarina (UFSC), Florianópolis, SC 88040-900, Brazil. 4.—e-mail: carlos.rambo@ufsc.br

This work reports the synthesis of $Ni(OH)_2$ aerogels incorporated *in situ* with polypyrrole (PPy) for application as electrodes in high-capacity energy storage devices. $Ni(OH)_2$ gels were prepared by the sol–gel method from $NiCl_2$ as precursor and propylene oxide as gelling agent in ethanol. Pyrrole monomer was added prior to gelling of the sol and *in situ* polymerized using ammonium persulfate as oxidant agent. After solvent exchanges from ethanol to acetone, the gels were dried in a CO_2 supercritical point drier. Powdered aerogels were deposited onto both sides of a poly(vinyl alcohol)/H_3PO_4 film (electrolyte/separator) and the contacts were closed with copper foils, resulting in a complete device. Through cyclic voltammetry and charge/discharge curves, the performance of the supercapacitors was evaluated by the specific capacitance, power and energy densities and series resistance. The specific capacitance was increased by 43% with the incorporation of 0.2 mol/L PPy (276 F/g) and the series resistance obtained decreased by 79% (46.5 Ω/cm^2), which reflects the enhanced performance and electrochemical properties of $Ni(OH)_2$ aerogel- based devices incorporated with PPy.

Key words: $Ni(OH)_2$ aerogels, polypyrrole, supercapacitors, nanocomposites

INTRODUCTION

Nowadays, various applications, such as electronic devices, electric vehicles, and portable equipment, require efficient energy storage systems. Supercapacitors offer a combination of high power density and high energy density, which are required for small, low-weight devices, capable of storing charge in the order of hundreds of F/g.

Many metal oxides and composites have excellent electrochemical properties to create supercapacitors. However, industrial applications of those materials are complex due to high processing costs, operating voltage, and toxicity.[1] Transition metals are quite promising for use in supercapacitors. For instance, ruthenium oxide (RuO_2) can reach high specific capacitances of around 1500 F/g, but its high cost and its shortage in nature makes it unattractive.[2] Alternatively, manganese oxide (MnO_2) has a high energy density, low cost and abundance in nature; however, its capacitance ranges from 50 F/g to 250 F/g because it presents a fast charge/discharge rate and low conductivity. Both nickel oxide (NiO) and nickel hydroxide ($Ni(OH)_2$) are of great interest for electrochemical applications as they feature a good cost–benefit ratio and high pseudo-capacitive performance,[1,3] typically characterized by faradaic redox peaks in cyclic voltammograms (CV) curves. $Ni(OH)_2$ is a starting material for NiO, which is formed after calcination.[4] $Ni(OH)_2$ is usually applied as electroactive materials in biosensors,[5] electrochemical capacitors,[6] batteries,[7] photocatalysis,[8] electro-catalysis, and electro-synthesis,[9] as well as

(Received October 17, 2016; accepted April 11, 2017; published online April 28, 2017)

in electrochemical sensors.[10] Xu et al.[11] produced core–sheath-structured Ni-$Ni(OH)_2$ nanowire membranes for electrochemical energy storage electrodes with a high volumetric capacity and an excellent rate capability.

To ensure high electrochemical activity of the electrodes, despite low crystallinity, a large concentration of defects in the structure and high surface area are also desired. The combination of the sol–gel process with the supercritical drying process results in highly porous materials with a high specific surface area (aerogels) which amplifies the ion transport through the mesoporous network. The control of such nanostructures allows the use of aerogels in electrochemical processes.[12]

To improve the mechanical resistance, conductivity and reversibility in the charge/discharge process, many studies have been reported regarding the incorporation of other materials to form hybrid electrodes.[13] In this sense, the application of conductive polymers in supercapacitors is attractive because of their high charge density, low cost, and intrinsic conductivity. The most investigated conductive polymers for application in supercapacitors are polypyrrole, polyaniline, and polythiophene.[14–16] Han et al.[17] reported a hybrid device formed by manganese oxide, polypyrrole, and graphene nanosheets (MnO_2/PPy/rGO) with 404 F/g in 0.25 mA/g. In another work, iron oxide and polypyrrole (Fe_2O_3/PPy) composites exhibited a specific capacitance of 420 F/g.[18] Murugan[19] showed an increase of 40–300 F/g with the incorporation of poly(3,4-ethylenedioxythiophene) (PEDOT) in the structure of molybdenum oxide (MoO_3). Although the majority of supercapacitors use liquid electrolytes, this can be disadvantageous regarding the possibility of leakage during operation, resulting in a performance decrease.[20]

In recent years, flexible solid-state supercapacitors have been developed using gels as electrolytes as promising portable energy storage devices, mainly because of their high power density, long life cycle, environmental compatibility, flexibility, and stability.[21,22]

In this work, nanostructured composites composed of $Ni(OH)_2$ aerogels incorporated *in situ* with polypyrrole were produced and applied as electrodes in supercapacitors.

EXPERIMENTAL

For the synthesis of aerogels and composites, nickel chloride hexahydrate ($NiCl_2{\cdot}6H_2O$; Vetec) was used as the $Ni(OH)_2$ precursor. Pyrrole monomer (Py; Sigma-Aldrich) was used for *in situ* polymerization. Py was distilled under vacuum and stored in a refrigerator at 8°C to avoid pre-polymerization. Ammonium persulfate (APS; Vetec) was employed as an oxidant agent and used as-received. Poly(vinyl alcohol) (PVA, 98–99% hydrolyzed; Sigma-Aldrich), phosphoric acid (H_3PO_4, 85%; Vetec), ethanol (ETOH, 99.5%; Synth), propylene oxide (99%), and acetone (99.9%) were used for the synthesis.

Aerogels of $Ni(OH)_2$ incorporated with different concentrations of PPy were synthesized. For nickel hydroxide alcohol gel synthesis, a solution with 0.37 g of $NiCl_2{\cdot}6H_2O$ in 2.5 ml of ETOH was prepared and stirred until complete dissolution. Then, 1.8 ml of propylene oxide was added under constant agitation. For the synthesis of $Ni(OH_2)$/PPy aerogels, Py was added together with 0.37 g of $NiCl_2{\cdot}6H_2O$ in 2.5 ml of ETOH. Afterwards, propylene oxide and the oxidant agent (APS) were added. Different concentrations of Py (0.2 mol/L and 0.4 mol/L) and ammonium persulfate (0.03 g and 0.06 g) at a ratio of 0.18 of oxidizing agent/monomer were prepared. The solution was poured into molds and left for 24 h under ambient conditions, which resulted in rigid light green opaque gels. The gels were immersed in a bath of ETOH for 1 day and, during the next 4 days, the ETOH was gradually replaced by acetone. The samples were then dried in a CO_2 critical point dryer (SPI-Dry E3100), in which acetone was slowly replaced for CO_2 during 5 days. The aerogels were submitted to a heat treatment at 200°C for OH-groups removal.

The electrolyte/separator was prepared according to Fei et al.[23] A solution containing 6 g of PVA, 6 g of H_3PO_4 and 60 ml of distilled water was stirred under heating to 85°C until complete dissolution and subsequently poured into a Petri dish. The formed film was left at ambient conditions to evaporate the excess of water.

The supercapacitor was assembled in a sandwich-like symmetric device, in which the aerogel powder was deposited on both sides of the film (electrolyte/separator) and between copper foil contacts.

X-ray diffractometry was applied for phase identification (XRD; Phillis, X-Pert) using a Cu Kα radiation (λ = 1.54 Å). Powdered aerogels were placed on aluminum stubs and scanned over a 2θ interval between 5° and 90° in 1°/min steps. The specific surface area was determined by a multipoint B.E.T. surface area (NOVA 1200e; QuantaChrome) through nitrogen adsorption–desorption isotherms. Raman spectroscopy (InnoRam, B&W TEK) was also performed for structural analysis. The morphology and nanostructure of the composite aerogels were evaluated by transmission electron microscopy (TEM;, JEM-1011) operating at 100 kV. The mean size of the nanoparticles was obtained from the analysis of magnified TEM images.

CV, and galvanostatic charge/discharge were carried out using a high precision SMU (Agilent B2912A). Cyclic voltammetry was measured in a range from −1 V to 1 V with 1 M H_3PO_4/PVA as electrolyte. Voltammetry was performed with different scanning rates (5 mV/s, 10 mV/s, 25 mV/s, 50 mV/s, 75 mV/s, and 100 mV/s). The capacitance of the devices was obtained through the area of the voltammogram, according to Eq. 1. The specific capacitance (F/g) was calculated from the ratio of

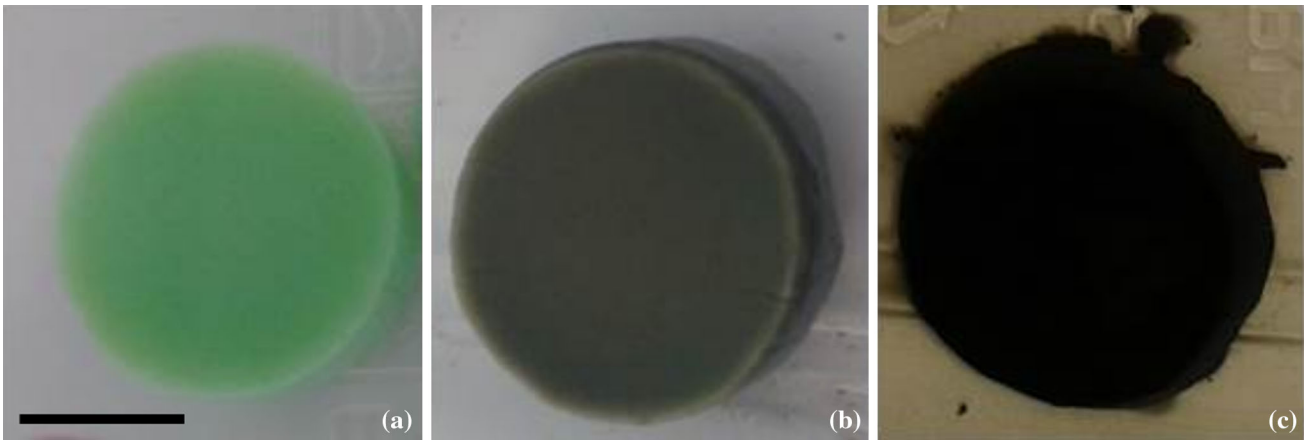

Fig. 1. The aerogels: (a) $Ni(OH)_2$; (b) $Ni(OH)_2$/PPy-0.2; (c) $Ni(OH)_2$/PPy-0.4. Bar 5 mm.

capacitance (in F) through the mass of the electrodes.[24] Cycle stability was evaluated after 1000 cycles at a scanning rate of 100 mV/s. To analyze the charge/discharge curves, the galvanostatic method was applied. For galvanostatic measures, the current density used was 10 mA/g or 50 mA/g. From these curves, it was possible to calculate the energy density (E), the equivalent series resistance (ESR) and the power density (P) of the device, according to Eqs. 1 to 3[25]:

$$E = \frac{C \times \Delta V^2}{2} \quad (1)$$

$$\mathrm{ESR} = \frac{iR_{\mathrm{drop}}}{2 \times I} \quad (2)$$

$$P = \frac{I \times \Delta V}{2 \times m_{\mathrm{ac}}} \quad (3)$$

where: C = capacitance; I = discharge current; m_{ac} = mass of the active material (aerogel); ΔV = potential after complete charge; iR_{drop} = difference between the extremes during charge and discharge.

RESULTS AND DISCUSSION

The obtained aerogels exhibited similarities to those synthesized by Gash et al.[26] presenting a greenish coloration (Fig. 1a). According to Rolison et al.,[12] the incorporation of conducting polymers after gelation of metal oxide alcohol gels results in poor electrochemical properties, as there is a non-homogeneous distribution of the polymer. On the other hand, for incorporation during gelation, the polymer reaches a homogenous distribution due to microstructural control. In this way, pyrrole was incorporated during the gelation process. The limitation for the incorporation of PPy, and consequently in the modification of its properties, is the inability of oxidation and gelation of the alcohol gel with a high content of the conducting polymer. The aerogels incorporated with the conducting polymer exhibited the same texture, but with higher fragility and featured a gray color as shown in Fig. 1. With the increase in the concentration of the conducting polymer, the color of the aerogel became darker (dark gray), as shown in Fig. 1b and c.

Figure 2a shows the x-ray diffractograms of a $Ni(OH)_2$ aerogel and the nanocomposites of $Ni(OH)_2$ incorporated with 0.2 mol/L and 0.4 mol/L PPy. The spectra of $Ni(OH)_2$ and $Ni(OH)_2$ (200°C) aerogels are characteristic for an amorphous phase, with a halo centered at around $2\theta = 14°$, which is related to the (001) planes of a α-$Ni(OH)_2$ structure.[27] The spectrum of the $Ni(OH)_2$ aerogel also exhibits halos at $2\theta = 36°$ (110)/(111) and at $2\theta = 60°$ (301), quite similar to the aerogel of $Ni(OH)_2$ synthesized by Gash et al.[26] For the composites incorporated with different concentrations of PPy, the peak at $2\theta = 20.7°$ is related to the β-$Ni(OH)_2$ structure, and the peaks at $2\theta = 35.5°$, and $2\theta = 59.1°$ correspond to α-$Ni(OH)_2$. According to Bora et al.,[28] the peak relative to pure amorphous PPy is centered at $2\theta = 24.65°$, which overlaps the (001) peak. After PPy incorporation, there is an intermediate structure between α- and β-$Ni(OH)_2$ as a result of hydration and incorporation of impurities, which can further influence the performance of the electrode.[29]

Figure 2b presents Raman spectra for aerogels incorporated with different concentrations of Py, in which two typical peaks were observed. For pure PPy, the characteristic bands were observed at 1383 cm^{-1} and 1570 cm^{-1} due to the ring stretching mode e and the C=C backbone stretching of PPy, respectively.[30] The incorporation of the conducting polymer resulted in changes in the characteristic peaks (1374 cm^{-1} and 1554 cm^{-1}) for the composite with the lower concentration of PPy, ($Ni(OH)_2$/PPy-0.2). A small shift occurred, probably related to $Ni(OH)_2$. With the increase in concentration, this

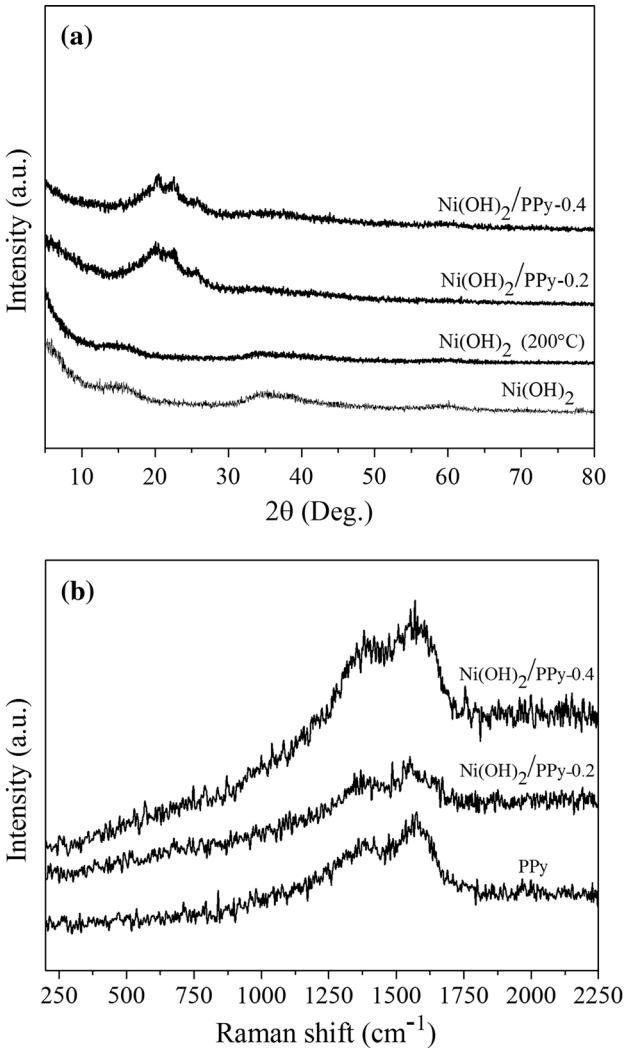

Fig. 2. Structural analyses of the $Ni(OH)_2$-based nanocomposites: (a) XRD spectra; (b) Raman spectra.

shift is not observed. In the case of ring deformation (deprotonated pyrrole), peaks in the region of 1040–1160 cm^{-1} would be revealed.[31] In this way, it is possible to state that the polymerization occurred as expected.

Figure 3 shows TEM micrographs of $Ni(OH)_2$ aerogels synthesized at ambient temperature and heat-treated at 200°C and $Ni(OH)_2$/PPy composites polymerized with different concentrations of Py. The $Ni(OH)_2$ aerogel (Fig. 3a) exhibits a typical porous network structure composed of interconnected spherical particles with sizes in the range of 25–35 nm. After calcination of $Ni(OH)_2$ at 200°C (Fig. 3b), it can be observed that the particles maintained their spherical structure but with a greater volume of pores. This behavior was not observed for $Ni(OH)_2$ aerogels incorporated with PPy (Fig. 3c and d). It can be noticed in the $Ni(OH)_2$/PPy-0.2 composite that, with the polymerization of Py, the aerogel nanoparticles remain interconnected, though reducing their spherical shape. With the increase of the concentration to 0.4 mol/L of Py in the composite, a less porous structure is generated with interconnected spherical-shaped coalesced particles. This behavior can be explained by the polymerization of the conducting polymer on the nanoparticles in smaller pores.[32]

During calcination, the hydroxyl groups are removed, which causes important changes in the structure of the aerogel depending on the temperature at which it is submitted. Up to 200°C, the pores of the structure still remain, but the hydroxyl groups were totally removed.

Table I presents the results of the B.E.T. analysis of $Ni(OH)_2$ aerogels and of the nanocomposites. Usually when the structure has a low crystallinity, as is the case with $Ni(OH)_2$, it is possible to obtain a higher specific surface area than its high-crystallinity counterpart.[33] On the other hand, after calcination at 200°C, significant crystallization has not yet occurred but hydroxyl groups are removed, resulting in a specific surface area of 200.5 m^2/g and an average volume of pores of 0.22 cm^3/g. For the $Ni(OH)_2$/PPy composites, as the concentration of the conducting polymer increased, the surface area decreased (from 109.81 m^2/g to 80.56 m^2/g), as did the average pore volume (from 0.19 cm^3/g to 0.14 cm^3/g). These values are expected because of the incorporation of the conducting polymer between the particles of the aerogel, corroborating the TEM analysis. It is known that the surface area influences the capacitance of the material. Highly porous materials with a high surface area facilitate ion transportation through the solid network, a characteristic that enhances the charge storage capacity.[12]

The cyclic voltammetry of $Ni(OH)_2$ aerogels at ambient temperature, calcined at 200°C, and of the $Ni(OH)_2$/PPy composites with different concentrations of PPy are shown in Fig. 4. A peak characteristic of the redox reaction can be observed in devices composed only with $Ni(OH)_2$ (Fig. 4a and b). A positive peak near 0.30 V indicates the oxidation of $Ni(OH)_2$ and the negative peak near 0.31 V indicates a reduction process.[34] The same voltammogram behavior was reported by Patil et al.[4] for β-$Ni(OH)_2$. Moreover, for the devices incorporated with PPy (Fig. 4c and d), two characteristic peaks are present: one for PPy and the other for $Ni(OH)_2$. These nanoparticles are also excellent conductors of electrons with low equivalent resistance, demonstrated by the alteration of the shape of the curves of VC with the increase of the scan rate from 1 mV/s to 100 mV/s. The anode and cathode peaks, however, shifted with increasing scan rate, because of the internal resistance of the electrode.[35] In comparison, Fig. 4e displays the cyclic voltammetry curves of all devices at the same scan rate (100 mV/s), where incorporation of PPy is clearly verified by the presence of its redox peaks.

In Fig. 5a, changes can be observed in the specific capacitance for voltammograms carried out with

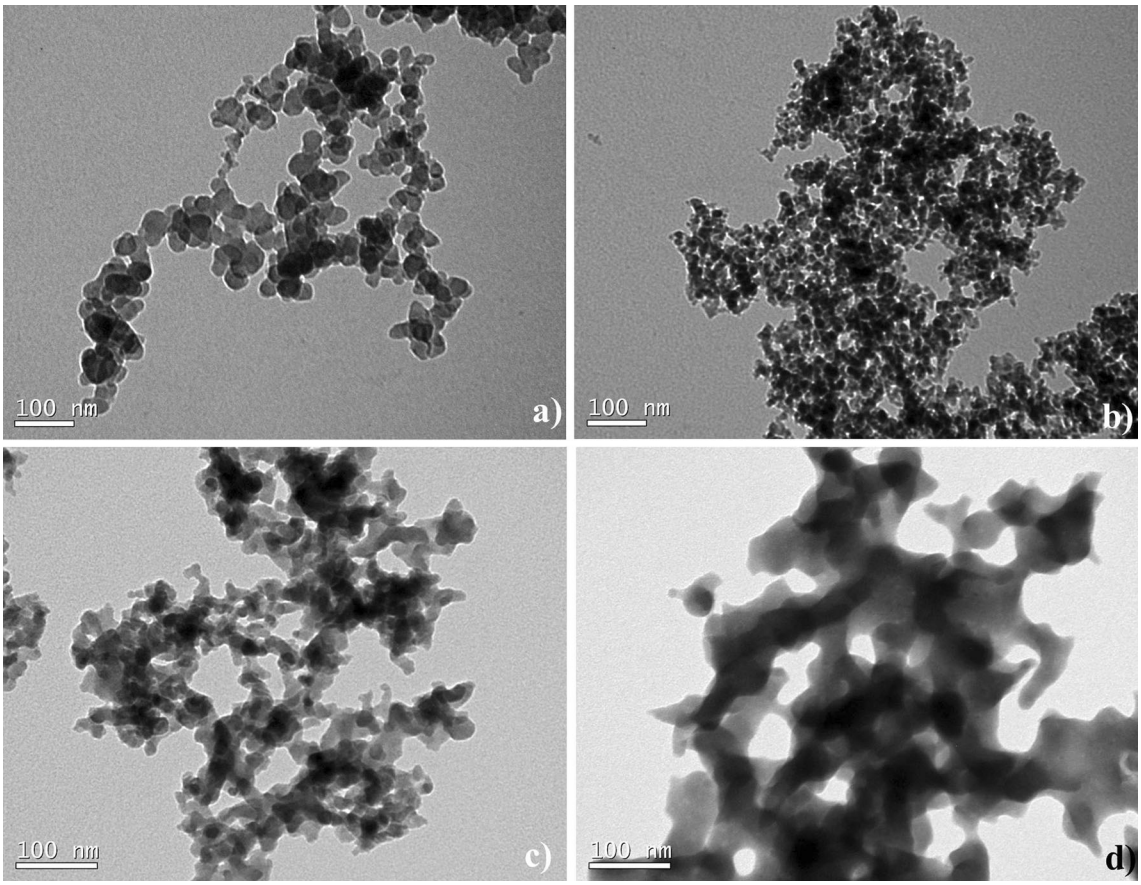

Fig. 3. TEM micrographs of the $Ni(OH)_2$-based nanocomposites: (a) $Ni(OH)_2$ aerogel at ambient temperature; (b) $Ni(OH)_2$ (200°C); (c) $Ni(OH)_2$/PPy-0.2; (d) $Ni(OH)_2$-0.4.

Table I. Specific surface area and pore volume of the $Ni(OH)_2$-based nanocomposites

Sample	Specific surface area (m^2/g)	Pore volume (cm^3/g)
$Ni(OH)_2$	173.6	0.18
$Ni(OH)_2$ (200°C)	200.5	0.22
$Ni(OH)_2$/PPy 0.2	109.8	0.19
$Ni(OH)_2$/PPy 0.4	80.6	0.14

different rates. The higher the scan rate, the less time the reactions have to occur, resulting in a lower charge transfer as well as increased current levels. The change in capacitance with dissimilar scan rates indicates that the capacitance is based on redox reactions.[36] The highest specific capacitance occurred for the lowest rate (5 mV/s). This behavior reveals the capacitive contribution of the faradaic process, because the total value of the capacitance of a supercapacitor is the combination of the effect of the double layer and the pseudocapacitance.[37] With the increase of the scan rate, the specific capacitance decreases gradually, which can be attributed to the ion diffusion of the electrolyte and the migration to the active electrodes at low scan rates. For high scan rates, the effect of the diffusion can limit the migration of these ions, causing some active surfaces to become inaccessible for charge storage. Figure 5b shows the specific capacitance related to the surface area for the devices with $Ni(OH)_2$ electrodes (ambient temperature and treated at 200°C) with different concentrations of PPy. It can be seen that the surface area contributes to an increase in specific capacitance. The incorporation of the conducting polymer on the structure of the $Ni(OH)_2$ aerogel enhances the electrical conductivity of the electrodes. For the composite with a higher amount of Py (0.4 mol/L), low capacitance and low specific surface area were recorded. This can be explained by the absence of reactivity of the oxygen present in the functional groups of the hydroxide to perform the redox reactions at the electrode/electrolyte interface.[38]

Figure 6 shows the cycle stability of the $Ni(OH)_2$ (200°C) aerogel and of the $Ni(OH)_2$/PPy-0.2 composite. After 1000 cycles, both of the devices exhibited good stability at 100 mV/s.[39] An increase of 18% in the capacitance of the $Ni(OH)_2$ device can be observed. This behavior is considered positive for

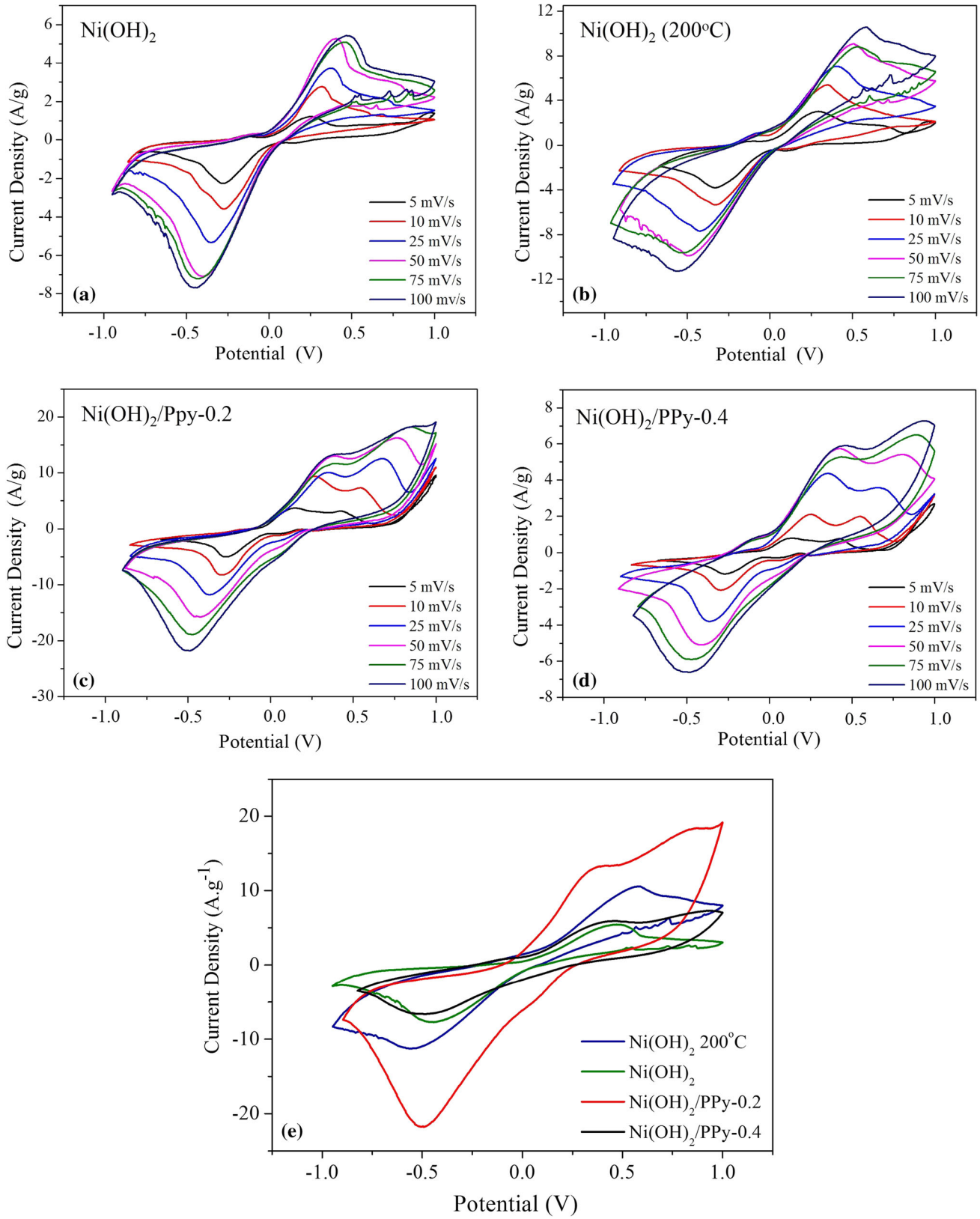

Fig. 4. Cyclic voltammetry of $Ni(OH)_2$-based aerogels: (a) $Ni(OH)_2$ aerogel at ambient temperature; (b) $Ni(OH)_2$ (200°C); (c) $Ni(OH)_2$/PPy-0.2; (d) $Ni(OH)_2$-0.4; (e) all composites at the same scan rate (100 mV/s).

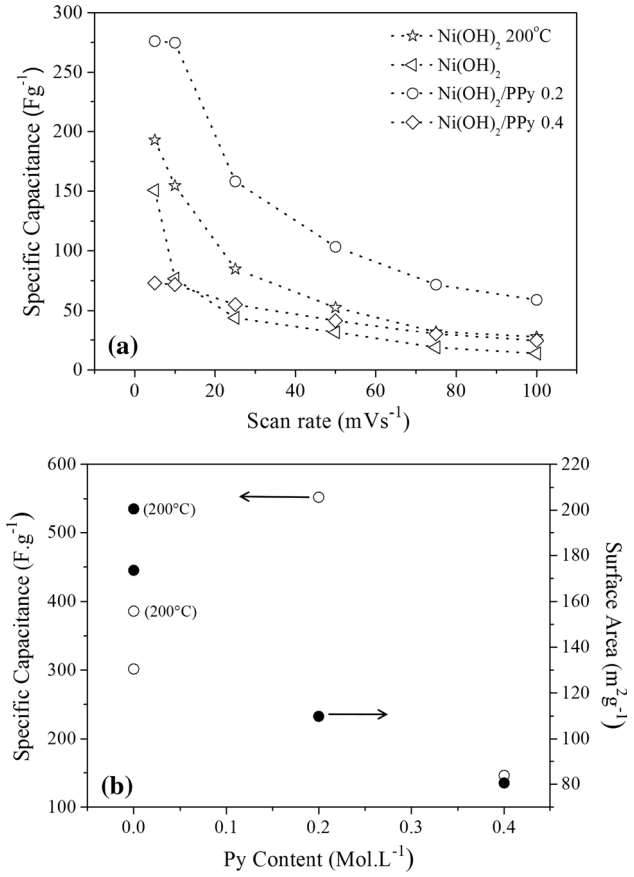

Fig. 5. Specific capacitance in function of: (a) scan rate and (b) Py concentration.

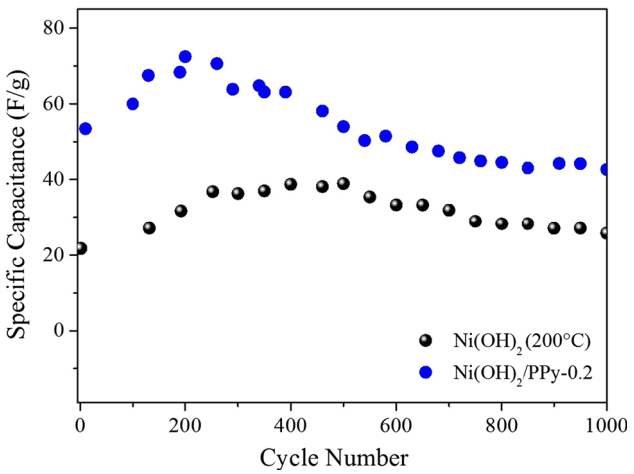

Fig. 6. Cycle stability of $Ni(OH)_2$ (200°C) and $Ni(OH)_2$/PPy-0.2.

devices based on faradaic processes.[40] Specific capacitance increased gradually up to 400 cycles, when the device is completely active.[41,42] The $Ni(OH)_2$/PPy-0.2 composite exhibits similar behavior, with an 80% retention of the initial capacitance. The slight capacitance reduction is a result of the structural alteration in electrodes and separator[43] and PPy dagradation.[44]

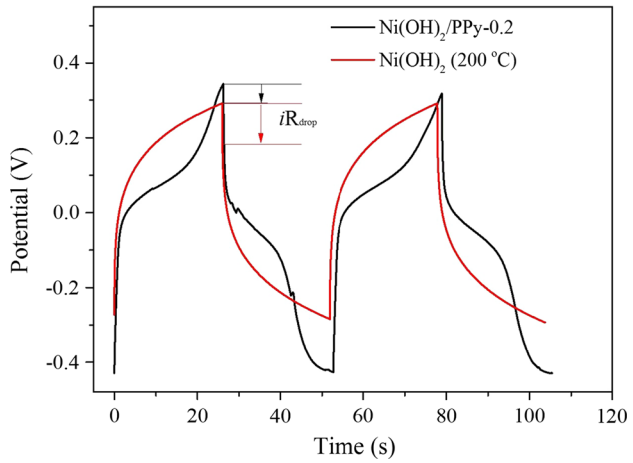

Fig. 7. Charge/discharge curves of $Ni(OH)_2$ (200°C) and $Ni(OH)_2$/PPy-0.2.

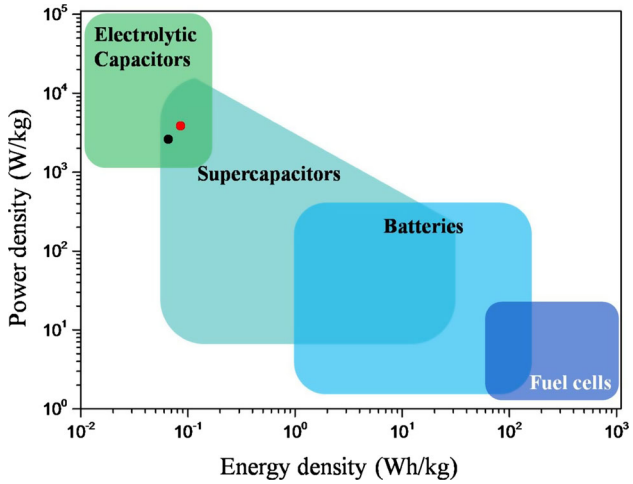

Fig. 8. Ragone chart containing the $Ni(OH_2)$ (200°C) and $Ni(OH_2)$/PPy-0.2 data.

For charge/discharge measurements (Fig. 7), devices with better results of capacitance were chosen: $Ni(OH)_2$ (200°C) and $Ni(OH)_2$/PPy-0.2. It can be observed that the curve corresponding to the aerogel of $Ni(OH)_2$/PPy-0.2 displays a non-linear behavior during charging and discharging, typical for faradaic electrode materials.[3] This effect indicates the contribution of pseudocapacitance, responsible for the largest specific capacitance presented in the voltammograms.[24] The ESRs were 221.8 Ω/cm^2 for $Ni(OH)_2$ (200°C) and 46.5 Ω/cm^2 for $Ni(OH)_2$/PPy-0.2. This property represents the intrinsic resistance of materials and contact resistance between them. The reduction of resistance in series after incorporation of PPy suggests the improvement of conductivity and a more efficient electron transfer between the electrolyte and the electrode.[45]

With respect to energy density and power density, the high values for the $Ni(OH)_2$/PPy-0.2 composite reflect its good performance and electrochemical properties.[39]

The Ragone chart containing the supercapacitors with $Ni(OH_2)$ (200°C) and $Ni(OH_2)$/PPy-0.2 is shown in Fig. 8. The energy density of the device with $Ni(OH_2)$/PPy-0.2 reached 0.064 Wh/kg and a power density of 2.92 kW/kg (black dot in the chart). These values are very close if compared with $Ni(OH)_2$ treated at 200°C (red dot: 0.084 Wh/kg and 3.95 kW/Kg, respectively).

CONCLUSIONS

PPy-incorporated $Ni(OH)_2$ aerogels were produced and tested as electrodes for high-capacity energy storage devices. PPy incorporation decreased the surface area, which was proportional to the PPy concentration. Through cyclic voltammetry and charge/discharge curves, the performance of the supercapacitors was evaluated by measuring specific capacitance, power and energy densities; series resistance was also determined. The specific capacitance was increased by 43% with the incorporation of 0.2 mol/L PPy (up to 276 F/g) and the series resistance obtained decreased by 79% (down to 46.5 Ω/cm^2). This reflects the highest performance and the best electrochemical properties of $Ni(OH)_2$ aerogel-based devices incorporated with PPy. The charge/discharge curves revealed the contribution of redox reactions from PPy, which resulted in higher energy and power densities.

ACKNOWLEDGEMENTS

The authors thank the National Council for Scientific and Technological Development (CNPq, Brazil) and the Coordination for the Improvement of Higher Level Personnel (CAPES/Brazil) for financial support. The Central Laboratory of Electronic Microscopy (LCME) at UFSC is also acknowledged.

REFERENCES

1. J. Gangwar, K.K. Dey, S.K. Tripathi, M. Wan, R.R. Yadav, R.K. Singh, Samta, and A.K. Srivastava, *Nanotechnology* 24, 415705 (2013).
2. T.Y. Wei, C.H. Chen, H.C. Chien, S.Y. Lu, and C.C. Hu, *Adv. Mater.* 22, 347 (2010).
3. W. Sun, X. Rui, M. Ulaganathan, S. Madhavi, and Q. Yan, Few-Layered $Ni(OH)^2$ Nanosheets for High-performance Supercapacitors. *J. Power Sources* 295, 323 (2015).
4. U.M. Patil, K.V. Gurav, V.J. Fulari, C.D. Lokhande, and O.S. Joo, *J. Power Sources* 188, 338 (2009).
5. A. Salimi, E. Sharife, A. Noorbakhsh, and S. Soltanian, *Electrochem. Commun.* 8, 1499 (2006).
6. Z. Li, Z. Zhou, G. Yun, K. Shi, X. Lv, and B. Yang, *Nanoscale Res. Lett.* 8, 473 (2013).
7. D.E. Reisner, A.J. Salkind, P.R. Strutt, and T.D. Xiao, *J. Power Sources* 65, 231 (1997).
8. J. Yu, Y. Hai, and B. Cheng, *J. Phys. Chem. C* 115, 4953 (2011).
9. Y.P. Gao, C.N. Sisk, and L.J. Hope-Weeks, *Louisa Chem. Mater.* 19, 6011 (2007).
10. Y. Fan, Z. Yang, X. Cao, P. Liu, S. Chen, and Z. Cao, *J. Electrochem. Soc.* 161, B201 (2014).
11. S. Xu, X. Li, Z. Yang, T. Wang, M. Xu, L. Zhang, C. Yang, N. Hu, D. He, and Y. Zhang, *Electrochim. Acta* 182, 464–473 (2015).
12. D.R. Rolison and B. Dunn, *J. Mater. Chem.* 11, 963 (2001).
13. G.A. Snook, P. Kao, and A.S. Best, *J. Power Sources* 196, 1 (2011).
14. A. Burke, *J. Power Sources* 91, 37 (2000).
15. W. Lei, L. Han, C. Xuan, R. Lin, H. Liu, H.L. Xin, and D. Wang, *Electrochim. Acta* 210, 130 (2016).
16. S. Konwer, R. Boruah, and S.K. Dolui, *J. Electron. Mater.* 40, 2248 (2011).
17. G. Han, Y. Liu, E. Kan, J. Tang, L. Zhang, H. Wang, and W. Tang, *RSC Adv.* 4, 9898 (2014).
18. M. Mallouki, F. Tran-Van, C. Sarrazin, P. Simon, B. Daffos, A. De, C. Chevrot, and J. Fauvarque, *J. Solid State Electrochem.* 11, 398 (2007).
19. A.V. Murugan, *J. Power Sources* 159, 312 (2006).
20. J.W. Kim and B.G. Choi, *Mater. Chem. Phys.* 159, 114 (2015).
21. L.F. Chen, X.D. Zhang, H.W. Liang, M. Kong, Q.F. Guan, P. Chen, Z.Y. Wu, and S.H. Yu, *ACS Nano* 6, 7092 (2012).
22. M.J. Tadjer, M.A. Mastro, J.M. Rojo, A.B. Mojena, F. Calle, F.J. Kub, and C.R. Eddy Jr., *J. Electron. Mater.* 43, 1188 (2014).
23. H. Fei, C. Yang, H. Bao, and G. Wang, *J. Power Sources* 266, 488 (2014).
24. K.W. Nam, W.S. Yoon, and K.B. Kim, *Eletrochim. Acta* 47, 3201 (2002).
25. H. Yu, L. Fan, Y. Lin, K. Xu, Z. Tang, C. Cheng, S. Tang, J. Lin, M. Huang, and Z. Lan, *J. Power Sources* 198, 402 (2012).
26. A.E. Gash, J.H. Satcheir, and R.L. Simpson, *J. Non-Cryst. Solids* 350, 145 (2004).
27. D.S. Hall, D.J. Lockwood, C. Bock, and B.R. Macdougall, *Proc. R. Soc. Lond. A.* 471, 1 (2015).
28. C. Bora and S.K. Dolui, *Polymer* 53, 923 (2012).
29. D.S. Hall, D.J. Lockwood, S. Poirier, C. Bock, and B.R. Macdougall, *J. Phys. Chem. A* 116, 6771 (2012).
30. S.P. Lim, A. Pandikumar, Y.S. Lim, N.M. Huang, and H.N. Lim, *Sci. Rep.* 4, 1 (2014).
31. D.K. Singh, S.K. Srivastava, A.K. Ojha, and B.P. Asthana, *Spectrochim. Acta A* 71, 823 (2008).
32. D. Muller, G.K. Pinheiro, T. Bendo, A.J.G. Aguayo, G.M.O. Barra, and C.R. Rambo, *J. Nanomater.* 2015, 169 (2015).
33. M.S. Wu, Y.A. Huang, C.H. Yang, and J.J. Jow, *Int. J. Hydrogen Energy* 32, 4153 (2007).
34. P. Simon, Y. Gogotsi, and B. Dunn, *Sci. Mag.* 343, 1210 (2014).
35. H.B. Li, M.H. Yu, F.X. Wang, P. Liu, Y. Liang, J. Xiao, C.X. Wang, Y.X. Tong, and G.W. Yang, *Nat. Commun.* 4, 1 (2013).
36. D.D. Zhao, S.J. Bao, W.J. Zhou, and H.L. Li, *Electrochem. Commun.* 9, 869 (2007).
37. Z. Fadakar, N. Nasirizadeh, S.M. BidokiIDOKI, Z. Shekari, and V. Mottaghitalab, *Micro Eng.* 140, 29 (2015).
38. Z. Wu, X.L. Huang, Z.L. Wang, J.J. Xu, H.G. Wang, and X.B. Zhang, *Scientific Reports* 4, 1 (2014).
39. D.P. Dubal, V.J. Fulari, and C.D. Lokhande, *Microporous Mesoporous Mater.* 151, 511 (2012).
40. H. Wang, C.M. Holt, Z. Li, X. Tan, B.S. Amirkhiz, Z. Xu, B.C. Olsen, T. Stephenson, and D. Mitlin, *Nano Res.* 5, 605 (2012).
41. L. Wang, X. Wang, X. Xiao, F. Xu, Y. Sun, and Z. Li, *Electrochim. Acta* 111, 937 (2013).
42. S. Shahrokhian, R. Mohammadi, and E. Asadian, *Int. J. Hydrogen Energy* 41, 17496 (2016).
43. Y. Su and I. Zhitomirsky, *Appl. Energy* 153, 48 (2015).
44. L.Q. Fan, G.J. Liu, J.H. Wu, L. Liu, J.M. Lin, and Y.L. Wei, *Electrochim. Acta* 137, 26 (2014).
45. G. Ma, M. Dong, K. Sun, E. Feng, H. Peng, and Z. Lei, *J. Mater Chem. A* 3, 4035 (2015).